GAUSSIAN SIGNAL DETECTION BY COPRIME SENSOR ARRAYS

Kaushallya Adhikari, John R. Buck *

University of Massachusetts Dartmouth
Electrical and Computer Engineering Department
North Dartmouth, Massachusetts, USA

ABSTRACT

Coprime sensor arrays (CSAs) achieve the resolution of a fully populated uniform linear array (ULA) with the same aperture using fewer sensors. The conventional CSA product beamformer suffers from a smaller array gain due to the reduced number of sensors. This paper derives that the conditional PDFs for detecting Gaussian signals in spatially white Gaussian noise with the CSA product processor are products of Bessel functions. The resulting ROCs are compared with those of the ULA energy detector for a conventional beamformer. The Bessel function CSA detection PDFs asymptotically converge to exponential distributions like the ULA detection PDFs, revealing that the detection gain of the nonlinear CSA processor is still proportional to the number of sensors. Monte Carlo simulations confirm the validity of the analytic results and the asymptotic approximations to the PDFs.

***Index Terms*— Coprime sensor array, ROC, signal detection**

1. INTRODUCTION

An array of sensors spatially samples propagating signals. A beamformer coherently combines the observed signal and incoherently averages the noise, increasing signal to noise ratio (SNR) at the output of the beamformer [1, 2]. The improvement in SNR due to the use of the beamformer is called array gain A_G and is defined as $A_G = SNR_O/SNR_I$, where SNR_O and SNR_I are the output SNR and the input SNR of the array, respectively [1]. The white noise array gain for an array is $||\mathbf{w}||^{-2}$, where $\mathbf{w}$ is the weight vector normalized such that the signal arriving from the look direction passes undistorted [1]. For a uniformly excited linear array, the white noise array gain is equal to the number of sensors in the array. Since a CSA has fewer sensors than its equivalent full ULA, a CSA processor has less ability to average white noise and hence is expected to have less array gain. This paper examines the detection performance of a CSA processor with the equivalent aperture full ULA when the arrays are operating in Gaussian signal and white Gaussian noise.

Section 2 explains CSA processing. Section 3 discusses the signal model and establishes the test statistics and their PDFs for the CSA and the full ULA. Section 4 plots and compares the region of convergence plots of the CSA and the full ULA and shows that the detection gain of the CSA processor is proportional to the number of sensors.

Conventions: Boldface lowercase math symbols denote vectors and boldface uppercase math symbols denote matrices. ^{H} denotes Hermitian. $a \sim \mathcal{CN}(\mu, \sigma^2)$ means a is a complex random variable with proper normal distribution with μ mean and σ^2 variance [3]. $a \sim \mathcal{N}(\mu, \sigma^2)$ means a is a real random variable with normal distribution with μ mean and σ^2 variance. $a \sim \mathcal{E}(\alpha)$ means a is a real random variable with exponential distribution with α mean and α^2 variance [4].

Subarray A has M_e sensors and undersampling factor N. Subarray B has N_e sensors and undersampling factor M. In the interest of brevity, we exploit metonymy by using the array (ULA or CSA) as shorthand for a specific beamformer processing the array data when it is clear from the context.

2. COPRIME SENSOR ARRAYS

A coprime sensor array (CSA) interleaves two aliased ULAs with undersampling factors N and M respectively where N and M are coprime [5–8]. Subarray A and Subarray B of a basic CSA have M and N sensors respectively and the subarrays share the first sensor as shown in Figure 1. Figure 2 illustrates the CSA processor. The CSA processor multiplies the conventionally beamformed Subarray A output with the complex conjugate of the conventionally beamformed Subarray B output that results in an estimate of the cross power spectrum of the input signal. The coprimality of the undersampling factors of the subarrays causes their grating lobes to be in different locations whereas their main lobes overlap completely. As a result, the CSA power spectrum has no grating lobes and has a main lobe with width the same as a full ULA with MN sensors. Hence, a CSA with $M + N - 1$ sensors has the same resolution as the full ULA with MN sensors. The CSA peak side lobe height is more than the full ULA. Adding sensors to the subarrays while keeping their intersensor spacings fixed reduces the peak side lobe height [5, 8]. This paper assumes that the numbers of sensors in the subarrays differ by one to

*Supported by ONR Basic Research Challenge Program grant N00014-13-1-0230.

minimize the total number of sensors [7] and the subarrays are extended to $M_e = 3M/2$ and $N_e = 3M/2 + 1$ sensors to reduce the peak side lobe height to half of the full ULA with equivalent aperture. The CSA with the added sensors in the subarrays is called extended CSA (ECSA). The full ULA with the equivalent aperture as the ECSA with $M_e = 3M/2$ and $N_e = 3M/2 + 1$ sensor subarrays has $3M/2 \cdot (M + 1)$ sensors.

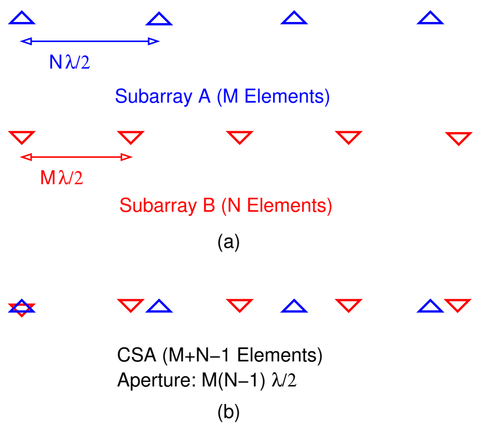

Fig. 1. a. Subarrays with $(M, N) = (4, 5)$ b. CSA for the subarrays in (a)

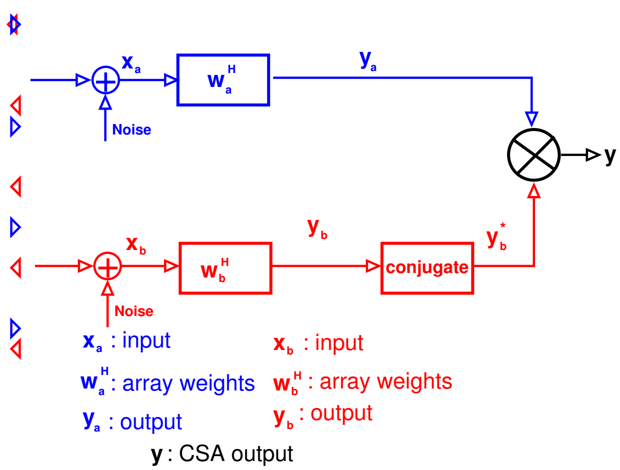

Fig. 2. The CSA processor multiplies the Subarray A (blue) and Subarray B (red) outputs resulting in the power estimate (black) from the look direction. (After Figure 2 of [8])

3. SIGNAL MODELS AND DETECTION TEST STATISTICS

This paper compares the detection performance of an ECSA with a standard ULA since the detection performance of a ULA has been well analysed. This section describes the signal model and establishes the test statistics for both the ECSA and the full ULA with the equivalent aperture.

3.1. Full ULA Signal Model and Test Statistic

Consider a ULA with L sensors and intersensor spacing $d = \lambda/2$, where λ is the wavelength of the signal of interest. The angle made by the input signal with the array axis is θ_s. Assume that the signal and noise are independent zero mean proper Gaussian random variables [3]. The input to the ULA is

$$\mathbf{x} = s\mathbf{v}_s + \mathbf{n}, \tag{1}$$

where $s \sim \mathcal{CN}(0, \sigma_s^2)$, $\mathbf{n} \sim \mathcal{CN}(\mathbf{0}, \sigma_n^2 \mathbf{I}_L)$. The signal component is $s\mathbf{v}_s$ and the noise component is $\mathbf{n}$. The L element vector $\mathbf{v}_s$ is the array manifold vector for direction θ_s. The i^{th} element of an array manifold vector for direction θ is $\exp(j\pi u(i-1))$ where $u = \cos(\theta)$. The output of the conventional beamformer (CBF) is $y = \mathbf{w}^H\mathbf{x}$, where $\mathbf{w} = \mathbf{v}_s/L$ is the weight vector. When the array is steered to the signal direction, the output of the beamformer for the signal model in (1) is $y = s + \mathbf{v}_s^H\mathbf{n}/L = s + \eta$, where $\eta = \mathbf{v}_s^H\mathbf{n}/L \sim \mathcal{CN}(0, \sigma_n^2/L)$.

The CBF detection statistic is the output power $t_u = |y|^2 = y_R^2 + y_I^2$, where y_R and y_I are the real and imaginary parts of the proper zero mean Gaussian random variable y, i.e. $y_R, y_I \sim \mathcal{N}(0, \sigma_s^2/2 + \sigma_n^2/(2L))$. Since y_R and y_I are independent normal random variables with zero mean and equal variance $\sigma_s^2/2 + \sigma_n^2/(2L)$, the random variable $t_u = y_R^2 + y_I^2$ has exponential distribution $f(t_u|H_1) = \mathcal{E}(\sigma_s^2 + \sigma_n^2/L)$ [4], where H_1 refers to the alternate hypothesis. In the signal absent case, t_u has exponential distribution $f(t_u|H_0) = \mathcal{E}(\sigma_n^2/L)$, where H_0 refers to the null hypothesis.

3.2. CSA Signal Model and Test Statistic

Consider a CSA with M_e and N_e element subarrays with undersampling factors N and M. The subarrays share $P = 2$ sensors when $M_e = 3M/2$ and $N_e = 3M/2 + 1$. Since each subarray is a ULA, the development of input and output models for the subarrays are similar to the full ULA in section 3.1. The outputs of the two subarrays are $y_a \sim \mathcal{CN}(0, \sigma_s^2 + \sigma_n^2/M_e)$ and $y_b \sim \mathcal{CN}(0, \sigma_s^2 + \sigma_n^2/N_e)$. The correlation coefficient ρ between y_a and y_b computed by substituting directly in the definition of correlation coefficient is

$$\rho = \frac{snr + \frac{P}{M_e N_e}}{\sqrt{\left(snr + \frac{1}{M_e}\right)\left(snr + \frac{1}{N_e}\right)}}, \tag{2}$$

where $snr = \sigma_s^2/\sigma_n^2$.

The CBF CSA test statistic is $t_c = |y_a| \cdot |y_b|$. Since, as shown above, the underlying Gaussian signals y_a and y_b are correlated random variables, their magnitudes $|y_a|$ and $|y_b|$

are correlated Rayleigh variables. The PDF $g(t_c)$ of the product of the two dependent Rayleigh variables is [9, 10]

$$\begin{aligned} g(t_c|H_1) =& \frac{4t_c}{\sigma_a^2\sigma_b^2(1-\rho^2)} \cdot I_0\left(\frac{2t_c|\rho|}{\sigma_a\sigma_b(1-\rho^2)}\right) \cdot \\ & K_0\left(\frac{2t_c}{\sigma_a\sigma_b(1-\rho^2)}\right), \end{aligned} \tag{3}$$

where $I_0(\cdot)$ and $K_0(\cdot)$ are the zeroth order modified Bessel functions of the first and second kind, respectively, and σ_a^2 and σ_b^2 are the variances at the outputs of Subarray A and Subarray B, respectively. Equation (3) is the alternate hypothesis PDF for the CSA. When there is no signal present in the environment, the subarray outputs are still correlated since they share P elements. However, for small P the correlation coefficient between the subarray outputs is negligibly small and the CSA test statistic approaches the product of two independent Ralyleigh variables resulting in the K-distribution PDF $g(t_c|H_0)$ given by [9, 10]

$$g(t_c|H_0) = \frac{4t_c}{\sigma_a^2\sigma_b^2} \cdot K_0\left(\frac{2t_c}{\sigma_a\sigma_b}\right). \tag{4}$$

4. RESULTS

This section derives the analytical expressions for receiver operation characteristics (ROC) for both the CSA and the full ULA with equivalent aperture using the PDFs derived in Section 3.

The probabilities of false alarm and detection in ULA are

$$P_{fa,u} = Pr(t_u > \gamma|H_0) = \exp\left(\frac{-\gamma}{\sigma_{u0}^2}\right)$$

and

$$P_{d,u} = Pr(t_u > \gamma|H_1) = \exp\left(\frac{-\gamma}{\sigma_{u1}^2}\right),$$

where γ is the threshold, and σ_{u0}^2 and σ_{u1}^2 are the full ULA output variances for null and alternate hypotheses respectively. The probabilities of false alarm and detection in CSA are

$$P_{fa,c} = Pr(t_c > \gamma|H_0) = \int_\gamma^\infty g(t_c|H_0)dt_c$$

and

$$P_{d,c} = Pr(t_c > \gamma|H_1) = \int_\gamma^\infty g(t_c|H_1)dt_c.$$

No closed form expression exists for the CSA P_d and P_{fa}, so they are obtained using numerical integration. The green dashed line in Figure 3 represents the full ULA ROC curve evaluated using the analytical expressions for $P_{fa,u}$ and $P_{d,u}$ while the black dashed-dot line represents the CSA ROC curve obtained by evaluating the expressions $P_{fa,c}$ and $P_{d,c}$ using global adaptive quadrature method of numerical integration with the PDFs in (3) and (4). Figure 3 compares the analytical ROC curves against the corresponding Monte-Carlo simulations curves obtained by generating $100,000$ samples of the array output and calculating the probabilities of detection and false alarm at each threshold level. The sensor SNR for the plots in Figure 3 is 0 dB and the coprime pair is $(8, 9)$. The full ULA has 108 sensors while the subarrays have 12 and 13 sensors, yielding 23 sensors for the CSA. The comparison of the analytical plots against the simulated ones confirms the accuracy of the analytical expressions for both full ULA and CSA.

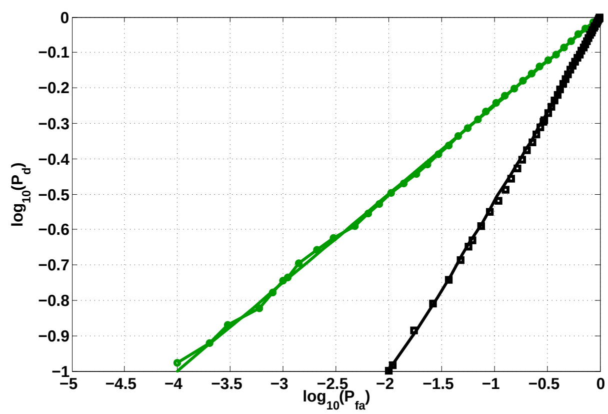

Fig. 3. Comparison of the ROC curves obtained from analytical expressions (green solid line for CSA and black solid line for CSA) and Monte-Carlo simulations (discrete circles for ULA and discrete squares for CSA) for full ULA and CSA.

Figure 4 compares the CSA and ULA ROC curves for coprime pairs $(M, N) = (12, 13)$ (red), $(8, 9)$ (green) and $(4, 5)$ (blue) where the SNR is 0 dB. The solid lines represent the ULA curves and the dashed-dot lines represent the CSA curves. For each coprime pair, the correpsonding ULA curve is above and to the left of the CSA curve confirming that the ULA has better detection performance than the CSA with the same resolution. Intuitively, this seems reasonable since the CSA has fewer sensors to average the uncorrelated white noise. Figure 4 also shows that the gap in the ROC curves for the ULA and the CSA increases as the coprime factors increase. This makes sense because as the coprime factors increase, the difference in the numbers of sensors between the CSA and full ULA also increases.

Asymptotic expansions of Bessel functions $I_0(\cdot)$ and $K_0(\cdot)$ [11, Page 920] reduce the alternate hypothesis PDF of

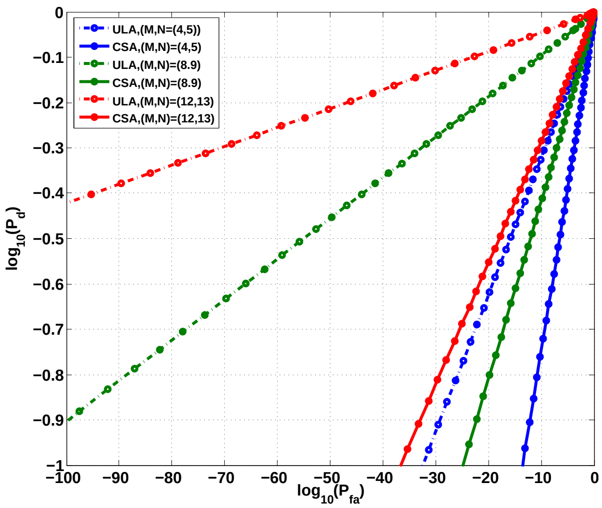

Fig. 4. Comparison of the detection performance of CSA and full ULA at equal SNR

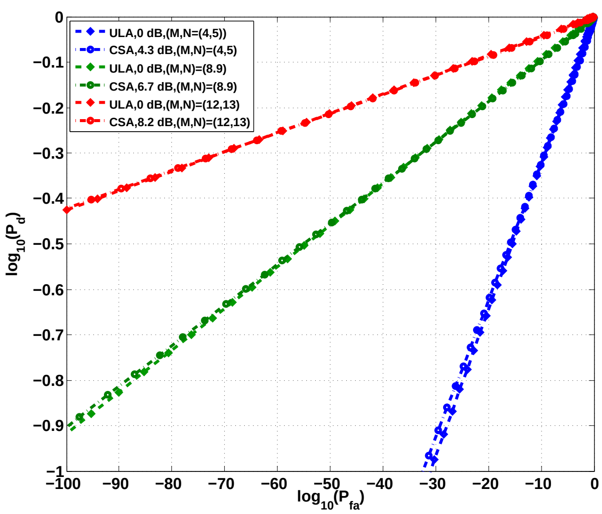

Fig. 5. Comparison of the detection performance of CSA and full ULA at different SNRs

CSA test statistic in (3) to

$$g(t_c|H_1) \approx \frac{1}{\sigma_a \sigma_b \sqrt{\rho}} \cdot \exp\left(\frac{-2t_c}{\sigma_a \sigma_b (1+\rho)}\right). \qquad (5)$$

Assuming high SNR and $M_e + N_e \approx 2M_e$ for large M_e, and plugging in the expression for ρ from (2), the PDF $g(t_c|H_1)$ is approximately $\mathcal{E}\left(\sigma_s^2\left(1 + \frac{1}{2M_e \cdot snr_c}\right)\right)$, where snr_c is the input SNR. The full ULA detection statistic has the PDF $\mathcal{E}\left(\sigma_s^2\left(1 + \frac{1}{L \cdot snr_u}\right)\right)$, where snr_u is the input SNR. If $snr_c = snr_u \cdot L/(M_e + N_e) \approx snr_u \cdot L/(2M_e)$, the CSA PDF converges to the full ULA PDF.

Figure 5 compares the full ULA and CSA ROC curves for different coprime pairs where the SNR for the CSA is $L/(M_e + N_e - 2)$ times the full ULA SNR. The dashed lines with diamonds represent the full ULA ROC curves all at 0 dB SNR. The full ULAs have 30 (red), 108 (green) and 234 (blue) sensors.The dashed-dot lines with circles are the CSA ROC curves at 4.3 dB SNR with coprime pair $(4, 5)$ (red), 6.7 dB SNR with coprime pair $(8, 9)$ (green) and 8.2 dB SNR with coprime pair $(12, 13)$ (blue). These CSAs have the same aperture as the full ULA with 30, 108 and 234 sensors respectively. When the input SNRs are equal, a full ULA performs better than a CSA with the equivalent aperture. If the CSA input SNR is increased by $L/(M_e + N_e - 2)$, the CSA detection performance matches that of the ULA, as shown in Figure 5. For example, a CSA with coprime pair $(4, 5)$ at 4.3 dB performs as well as the equivalent full ULA at 0 dB. This shows that even though the CSA employs a nonlinear product processor, the detection gain of a CSA product detector is still proportional to the number of sensors like the ULA detector.

5. CONCLUSION

This paper derives the exact PDFs for the CSA test statistics for both alternate and null hypotheses and finds the analytical ROC curves. This paper shows that the detection gain of the CSA is $10 \log_{10}$(Number of sensors) dB for large coprime pairs and large SNR and explains why the detection gain for the non-linear CSA product processor has the same dependence on the number of sensors as the linear CBF for a ULA.

6. ACKNOWLEDGEMENT

The authors would like to thank Kathleen E. Wage and Piya Pal for helpful conversations in the development of this paper.

7. REFERENCES

[1] H. Van Trees. *Optimum Array Processing (Detection, Estimation and Modulation Theory, Part IV)*. John Wiley and Sons, Inc., New York, 2002.

[2] D.H. Johnson and D.E. Dudgeon. *Array Signal Processing: Concepts and Techniques*. Simon & Schuster, 1992.

[3] P.J. Schreier and L.L. Scharf. *Statistical Signal Processing of Complex-Valued Data: The Theory of Improper and Noncircular Signals*. Cambridge University Press, 2010.

[4] A. Papoulis. *Probability, Random Variables, and Stochastic Processes*. Mc-Graw Hill, 1984.

[5] P.P. Vaidyanathan and P. Pal. Sparse sensing with co-prime samplers and arrays. *IEEE Transactions on Signal Processing*, 59(2):573 –586, February 2011.

[6] P.P. Vaidyanathan and P. Pal. Theory of sparse coprime sensing in multiple dimensions. *IEEE Transactions on Signal Processing*, 59(8):3592 –3608, August 2011.

[7] K. Adhikari, J.R. Buck, and K.E. Wage. Beamforming with extended co-prime sensor arrays. *2013 IEEE International Conference on Acoustics, Speech and Signal Processing (ICASSP)*, pages 4183–4186, May 2013.

[8] K. Adhikari, J.R. Buck, and K.E. Wage. Extending co-prime sensor arrays to achieve the peak side lobe height of a full uniform linear array. *EURASIP Journal on Advances in Signal Processing*, 2014. doi:10.1186/1687-6180-2014-148. In press.

[9] M.K. Simon. *Probability Distributions Involving Gaussian Random Variables: A Handbook for Engineers and Scientists*. International Series in Engineering and Computer Science. Springer, 2007.

[10] K.S. Miller. *Multidimensional Gaussian distributions*. SIAM series in applied mathematics. Wiley, 1964.

[11] I.S. Gradshteyn and I.M. Ryzhik. *Table of Integrals, Series, and Products*. Academic Press, 1900.